

Article

Effect of Nb Doping on the Electrical Contact Properties of AgNi Contact Materials

Jingqin Wang^{1,2,*}, Menghan Wang¹, Jing Chen³ and Guanglin Huang³

¹ State Key Laboratory of Reliability and Intelligence of Electrical Equipment, Hebei University of Technology, Tianjin 300130, China; m15831390293@163.com

² Provincial and Ministerial Co-Construction Collaborative Innovation Center on Reliability Technology of Electrical Products, Hebei University of Technology, Tianjin 300130, China

³ Wenzhou Juxing Electric Contact Technology Co., Ltd., Wenzhou 325062, China; jxcj@china-juxing.cn (J.C.); jxhgl@china-juxing.cn (G.H.)

* Correspondence: jqwang@hebut.edu.cn; Tel.: +86-022-60204354

Abstract: AgNi contact materials have received widespread attention with the acceleration of the process of replacing AgCdO contact materials. However, the practical applications of AgNi contact materials are limited due to its disadvantage of poor resistance to melting welding. Firstly, following the first principles of the density functional theory, we simulated and tested an interfacial model of AgNi doped with varying amounts of Nb. Next, we fabricated AgNi electrical contact materials. Subsequently, we conducted electrical contact tests. Finally, the impact of Nb doping on the arc erosion behavior of AgNi electrical contact materials was analyzed. The results indicate that, with an increase in Nb doping content, the electrical contact performance and the degree of arc erosion exhibit a trend of initially decreasing and then increasing, which aligns with the simulation results. The mean values of arc energy, arc duration, and welding force for the material doped with 4.55% Nb were 181.02 mJ, 9.43 mS, and 38.45 cN, respectively. Moreover, the anode is more responsive to changes in Nb content compared to the cathode. The introduction of Nb enhances the viscosity of the molten pool in the AgNi electrical contact. Furthermore, the mechanisms of grain boundary strengthening and solid solution strengthening by Nb improve the weld performance resistance of the contact.



Citation: Wang, J.; Wang, M.; Chen, J.; Huang, G. Effect of Nb Doping on the Electrical Contact Properties of AgNi Contact Materials. *Coatings* **2024**, *14*, 638. <https://doi.org/10.3390/coatings14050638>

Academic Editor: Alicia Esther Ares

Received: 25 April 2024

Revised: 14 May 2024

Accepted: 16 May 2024

Published: 17 May 2024



Copyright: © 2024 by the authors. Licensee MDPI, Basel, Switzerland. This article is an open access article distributed under the terms and conditions of the Creative Commons Attribution (CC BY) license (<https://creativecommons.org/licenses/by/4.0/>).

Keywords: AgNi electrical contact material; Nb-doped; arc erosion behavior; density functional theory

1. Introduction

As one of the core components in low-voltage electrical appliances, the physical and electrical properties of electrical contact materials directly determine the stability of low-voltage electrical equipment [1]. A AgNi contact material has good electrical and thermal conductivity, low and stable static contact resistance, fast arc movement, good ductility, and excellent processing performance. Therefore, in recent years, AgNi has become one of the most extensively researched and vigorously developed cadmium-free silver-based contact materials. At present, the Ni content in AgNi materials used in various AC and DC low-voltage control appliances is typically between 10% and 20%. However, in practical applications, AgNi electrical contact materials suffer from the drawback of poor resistance to fusion welding. This limitation significantly hinders the widespread application of AgNi contact materials [2]. With the acceleration of the process of replacing toxic AgCdO contact materials, AgNi contact materials have received widespread attention. In order to enhance the performance of electrical contact materials, broaden their applications, and enhance the operational safety and reliability of switching appliances, improving the overall performance of AgNi contact materials has become a pressing priority for the advancement of the field of electrical contacts [3].

Studies have shown that doping is one of the most important methods in enhancing the properties of AgNi contact materials. Considering that the electrical or processing performance characteristics of AgSnO₂ and AgNi are highly complementary, Xue Tian combined the two into a AgNi-SnO₂ material. He explored the sintering process of the material in detail, as well as the effects of particle size, morphology, and content of Ni powder on the sintering, sintering fusion organization, and properties of the material [4]. Hu Dekao et al. established an interfacial model of graphene-doped AgNi based on the first principles. They analyzed the mechanism of doping for AgNi contact materials and prepared graphene-doped AgNi contact materials using an in situ synthesis method [5]. Wang et al. conducted experimental research on the properties of a Ag/Ni contact material doped with W and WO₃ [6]. Aikun Li et al. investigated the effect of various carbon-based isomers (carbon nanotubes, graphene nanosheets, and graphite) on the microstructure and properties of AgNi contact materials. The results indicated that all the carbon isomers enhanced the resistance to soldering, with graphene nanosheets showing the best arc erosion performance [7].

AgNi electrical contact materials all generate electrical arcs during the opening and breaking processes. The contact surface undergoes a series of physical and chemical changes, such as melting, evaporation, and spattering, under the action of the arc [8]. The structure of AgNi contact materials without additives is very simple. It consists of two-phase composite materials composed of Ag and Ni, with Ag as the matrix phase and Ni as the reinforcing phase. Ag and Ni have a poor compatibility; even if the temperature exceeds the melting point of Ni (1453 °C), the two metals cannot dissolve in each other and maintain a two-liquid-phase coexistence state. Therefore, AgNi materials are often prepared by powder metallurgy [9]. In the arc root region, the instantaneous temperature can exceed 2000 °C. At this point, more Ni particles dissolve rapidly. When the arc extinguishes, Ni will re-precipitate and deposit in the Ag matrix, forming secondary Ni crystalline particles. With the increase in the number of opening and closing cycles, the original Ni particles continue to precipitate, forming a layer of fine Ni in the contact area. The strength of its bond with Ag significantly increases, enhancing the contact resistance and arc erosion performance [10–13].

Under the action of a high-temperature arc, Nb can be synthesized with Ni into high-temperature Nb-Ni alloys. The addition of Nb results in fine-crystal strengthening and diffusion strengthening. It can also facilitate the diffuse distribution of precipitates through precipitation induction and control of the cooling rate. This process enhances the strength and toughness of contacts in a wide range, thereby improving material performance [14]. Therefore, this study selected Nb as the dopant to investigate the impact of Nb content on the electrical contact properties of AgNi contact materials.

The research on doping to enhance the anti-melt welding performance of AgNi has long been a subject of great interest. However, experimental studies on doping to improve the performance of AgNi contact materials have been conducted using a “trial and error” approach, leading to inefficiencies in various aspects. This method involves high investment and low efficiency, and the screening of additives that can effectively enhance the properties of contact materials is quite arbitrary. Therefore, there is an urgent need to find an effective theoretical method to enhance the efficiency of doping to improve the properties of AgNi contact materials. In light of this, this thesis integrates simulation calculations and experimental verification based on the first principles of the density functional theory. The aim is to determine the optimal doping content by calculating and analyzing its electrical properties. This approach aims to offer a novel research method and concept for enhancing the performance of AgNi materials in contact applications.

2. Models and Calculation Methods

2.1. Models

Ni and Ag in AgNi alloys are almost immiscible with each other in the solid state, and the two-phase interface of AgNi materials needs to be analyzed from a microscopic

atomic point of view. Firstly, the Ag and Ni cell models were optimized to obtain the cell model structure with the lowest total energy. Subsequently, the optimized cell models were analyzed on the surface. Previous studies have indicated that, among the bonding configurations at the AgNi interface, Ag(110)/Ni(211) exhibits the highest interfacial bonding energy, making it the most stable option [15]. In addition, the number of atomic layers is too small to fully reflect the nature of the material, leading to low credibility. Conversely, an excessive number of atomic layers will result in high computational costs. After conducting the surface energy convergence test, it was determined that the Ag(110) surface should consist of 6 atomic layers, while the Ni(211) surface should comprise 3 atomic layers. This determination was made by balancing the credibility of the calculation results with the computational cost constraints. The degree of mismatch was reduced by employing the method of creating supercells to fulfill the criteria of less than 10% mismatch and a 15% Ni mass fraction. The mismatch degrees in the X and Y directions were 0.81% and 4.32%, respectively. In order to prevent interaction in the periodic direction of the interface model, a 15 Å vacuum layer was included in the Ag(110)/Ni(211) interface model. Ni can dissolve approximately 30% of Nb by mass fraction, while Ag can only dissolve 0.1%–0.5% of Nb. Moreover, the formation of an interstitial solid solution necessitates that the ratio of solute atoms' diameters to solvent atoms' diameters be less than 0.59. In conclusion, the AgNi interface is deemed the most suitable solution for the AgNi interface, and an interstitial solid solution is not required for the AgNi interface. After replacing the freely relaxing Ni atoms with Nb atoms in the AgNi interface, a model of the AgNi interface with different doping ratios can be obtained, as shown in Figure 1. As shown in Figure 1a, Ag atoms near the interface remain in a free relaxation state with Ni atoms to form an interface. Nb is easily soluble in Ni and almost insoluble in Ag, so Nb atoms replace Ni atoms at the interface in Figure 1a in different proportions to simulate the actual situation of the AgNi interfacial material, as shown in Figure 1b–d. From the atomic number of each atom in Figure 1, the atomic ratio corresponding to each model can be obtained. Based on the atomic weight of each element, the mass share of each element in its corresponding AgNi electrical contact material can be calculated, as shown in Table 1. In this paper, the nomenclature for Nb-doped AgNi electrical contact materials is derived from the mass ratio of Nb elements as presented in Table 1. For instance, if the mass of doped Nb constitutes 2.29% of the total contact mass, the material is denoted as AgNi-Nb(2.29).

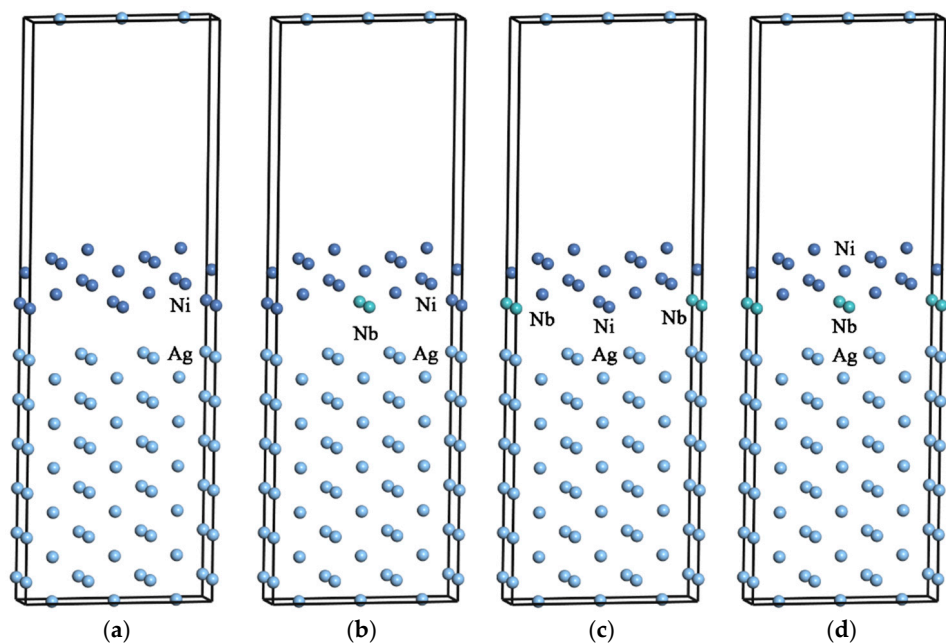


Figure 1. Modeling of the AgNi interface: (a) AgNi, (b) AgNi-Nb(2.29), (c) AgNi-Nb(4.55), and (d) AgNi-Nb(6.77).

Table 1. Atomic ratio, mass ratio of AgNi materials.

Material	Atomic Ratio	Mass Ratio
AgNi	75%:25%	84.65%:15.35%
AgNi-Nb(2.29)	75%:22.62%:2.38%	83.93%:13.78%:2.29%
AgNi-Nb(4.55)	75%:20.24%:4.76%	83.23%:12.22%:4.55%
AgNi-Nb(6.77)	75%:17.86%:7.14%	82.54%:10.69%:6.77%

2.2. Calculation Method

In this paper, the ultrasoft pseudopotential has been chosen to describe the interactions between valence electrons and ionic realities. The exchange–correlation energy is treated by the PBE (Perdew–Burke–Ernzerhof) generalization under the generalized gradient approximation, and the BFGS (Broyden–Fletcher–Goldfarb–Shanno) algorithm is used to simulate the different contents of the Nb-doped AgNi interface models with various levels of Nb doping [16]. The selected computational parameter settings are as follows: the truncation energy of the inverse easy space is set to 320 eV, the total energy for SCF self-consistent convergence is required to be less than 1.0×10^{-5} eV/atom, the average atomic stress should be below 0.5 eV/nm, the tolerance shift must be less than 0.02 nm, and the maximum stress deviation should not exceed 0.1 GPa. The simulation calculation parameter setting involves selecting the planar truncation energy and the K-point of the Brillouin zone. The larger the values of the truncation energy and the K-point, the smaller the calculation error, and the higher the credibility of the calculation’s results. However, this comes at the cost of a significant increase in the calculation period and the computational expenses. The smaller the values of the truncation energy and the K-point, the shorter the calculation period and the lower the calculation cost. However, this will lead to calculation errors and a decrease in the credibility of the results [17,18]. Therefore, convergence tests were conducted on the interface model, integrating the economic aspects of the calculation cost and the precision of the results to determine the parameter settings for the planar truncation energy and the K-point of the Brillouin zone, as shown in Table 2. The valence electron configurations considered for the calculations in this paper are Ag: $5s^14d^{10}$, Ni: $4s^23d^8$, Nb: $5s^14d^4$.

Table 2. Simulation parameter setting.

Parameters	Ag(110)	Ni(211)	AgNi Interface Model
Cut off energy/eV	517	400	517
Kpoint	$4 \times 3 \times 1$	$4 \times 3 \times 2$	$2 \times 9 \times 1$

3. Simulation Analysis

3.1. Interfacial Bond Strength Analysis and Wettability Prediction

The interfacial work of separation (W_{sep}) refers to the reversible work per unit area required to separate a two-phase interface into two free surfaces. This measurement is used to evaluate the interfacial bonding strength [19]. When the interfacial separation work is positive, it indicates that the two interfaces can form a stable interface. The larger the value of the separation work, the stronger the interfacial atomic bonding force and the higher the interfacial bonding strength. Conversely, when the interfacial separation work is negative, it indicates that the interface cannot exist stably.

The W_{sep} for AgNi is expressed as:

$$W_{sep} = (E_{Ag}^{slab} + E_{Ni}^{slab} - E_{AgNi}^{inter}) / A \quad (1)$$

where E_{Ag}^{slab} and E_{Ni}^{slab} represent the total energy of the Ag and Ni free surface systems, respectively; E_{AgNi}^{inter} represents the total energy of the relaxation interface system; and A represents the interface area.

The interfacial energy is the excess energy per unit area of the interface due to atomic distortion, chemical bonding changes, and structural strain at the interface during the formation of the interface in the system. It is used to evaluate the interfacial stability [20]. For interfaces composed of different solid-phase materials, the interfacial energy should be positive. The smaller the value, the higher the interfacial stability. The interfacial energy is calculated using the formula:

$$\gamma_{int} = \sigma_{Ag} + \sigma_{Ni} - W_{sep} \quad (2)$$

where σ_{Ag} and σ_{Ni} represent the surface energy of the free surfaces of Ag and Ni.

Among them:

$$\sigma = (E_{slab} - \frac{N_{slab}}{N_{bulk}} E_{bulk}) / 2A \quad (3)$$

In Equation (3), E_{slab} represents the total energy of the optimized surface model, E_{bulk} represents the total energy of the optimized cell model, N_{slab} represents the number of atoms contained in the surface model, and N_{bulk} represents the number of atoms contained in the cell model.

The total energy of the optimized interfacial model, the lattice constants a and b , which are required for calculating the interfacial area, and the interfacial work of separating AgNi before and after doping, obtained from the simulation calculations using Equation (1), are presented in Table 3. Table 4 displays the interfacial energy of AgNi before and after doping, calculated by substituting the results of simulation calculations into Equations (2) and (3).

Table 3. Interface separation work.

Doping Ratio	E_{Ag}^{slab} (eV)	E_{Ni}^{slab} (eV)	E_{AgNi}^{inter} (eV)	A (\AA^2)	W_{sep} ($\text{eV}/\text{\AA}^2$)
AgNi	−144,207.32	−16,423.96	−160,632.93	36.36	0.045
AgNi-Nb(2.29)	−144,207.32	−16,520.62	−160,729.58	33.78	0.049
AgNi-Nb(4.55)	−144,207.32	−16,734.64	−160,943.78	35.78	0.051
AgNi-Nb(6.77)	−144,207.32	−16,497.87	−160,706.91	36.59	0.047

Table 4. Interface energy.

Doping Ratio	σ_{Ag} (eV)	σ_{Ni} (eV)	γ_{int} ($\text{eV}/\text{\AA}^2$)
AgNi	0.038	0.150	0.143
AgNi-Nb(2.29)	0.038	0.132	0.121
AgNi-Nb(4.55)	0.038	0.128	0.115
AgNi-Nb(6.77)	0.038	0.147	0.138

According to the data in Tables 3 and 4, the interfacial separation work and interfacial energy are both positive. This suggests that the AgNi interfacial models, both before and after doping, can form stable interfaces. The interfacial separation work after doping has a larger value than that of the undoped AgNi, indicating that the interfacial atoms are more strongly bound to each other, and the interfacial bonding strength is higher after doping. The magnitude of their interfacial separation work is in the order of AgNi-Nb(4.55) > AgNi-Nb(2.29) > AgNi-Nb(6.77) > AgNi. This indicates that the addition of Nb can effectively enhance the interfacial bonding strength of AgNi. However, the interfacial bonding strength of the AgNi model begins to decrease with a further increase in Nb content. From the interfacial energy in Table 4, it can be seen that the addition of dopant atoms increases the stability of the interface. The stability is enhanced when Nb is doped by 4.55%. The interfacial bond strength and interfacial stability can predict the wetting performance of the contact material and, consequently, its electrical contact performance. The higher the interfacial bond strength, the stronger the interfacial stability, and the better the material's wettability. In practical applications, contact materials with better

wettability can dissolve more Ni particles in the Ag melt pool under the arc's influence. This process forms a uniformly dispersed alloy, enhances the viscosity of the melt pool, reduces spattering loss due to arc erosion, and contributes to improving the performance of the AgNi contact material. Therefore, the simulation results predict that Nb doping can improve the wettability and electrical contact properties of AgNi. However, as the doping content increases, the degree of improvement exhibits a pattern of initial enhancement followed by a decline.

3.2. Mechanistic Analysis of Interfacial Bond Strength

The density of states can reflect the interaction of individual atoms, as well as doped atoms, with other atoms in the interface model. It allows us to obtain the distribution pattern of electrons at different energy values [21]. The total density of states (TDOS) indicates the energy distribution state of all the electrons in the system, while the fractional wave density of states indicates the bonding of electrons in different orbitals. Figure 2 shows the density of states of AgNi before and after doping. Panel (a) displays the density of states of AgNi, while panels (b), (c), and (d) show the density of states of AgNi-Nb doped with different contents, respectively.

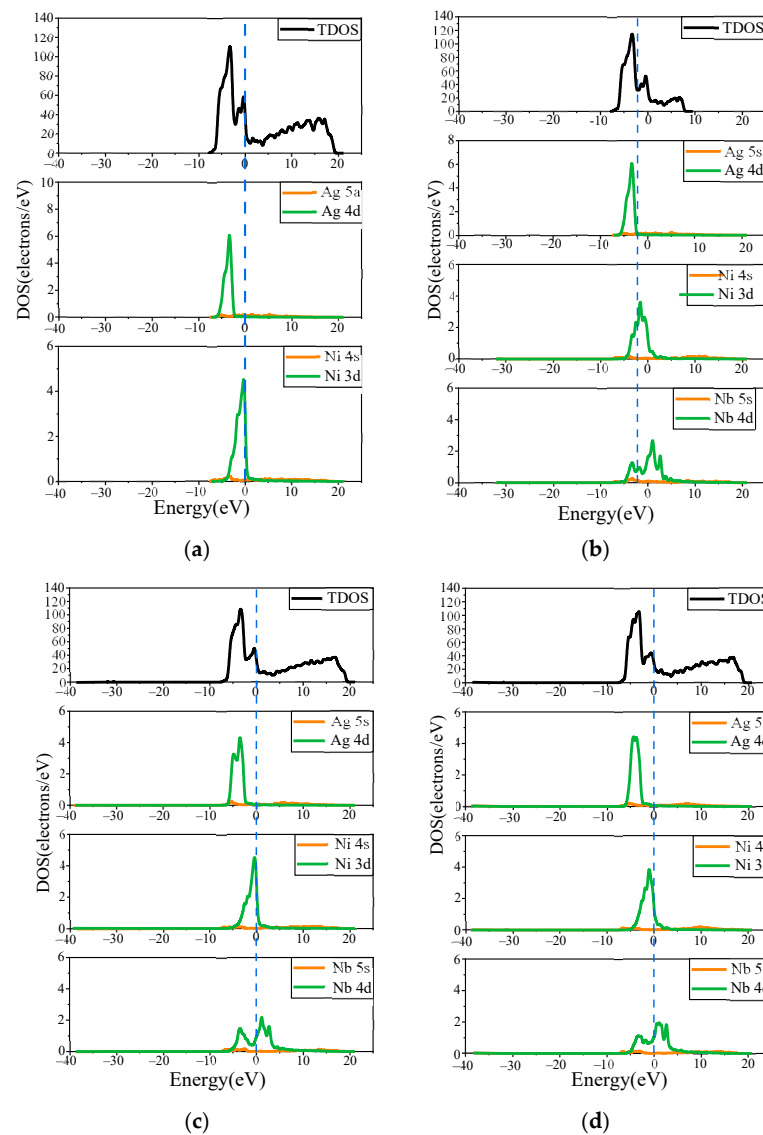


Figure 2. Density of states: (a) AgNi, (b) AgNi-Nb(2.29), (c) AgNi-Nb(4.55), and (d) AgNi-Nb(6.77).

From the density of states of AgNi in Figure 2a, it can be observed that the number of electrons near the Fermi energy level is higher, suggesting that AgNi exhibits a good conductivity. At $-7\text{ eV}\sim 0\text{ eV}$, the wave peaks of AgNi mainly originate from the d-orbitals of Ag elements and the d-orbital contributions of Ni elements. There are obvious overlapping peaks between the Ag-d orbitals and Ni-d orbitals in the range of $-5\text{ eV}\sim -3\text{ eV}$.

From the density of states of Nb(2.29)-doped AgNi in Figure 2b, it can be seen that there are clearly overlapping peaks between Ag-d and Ni-d orbitals and Nb-d orbitals at $-5\text{ eV}\sim -2\text{ eV}$, i.e., two-by-two hybridization for bonding orbitals, which produces interactions, and the Ni-d orbitals continue to hybridize with Nb-d at $-2\text{ eV}\sim 2\text{ eV}$. In the region of $0\text{ eV}\sim 7\text{ eV}$, the wave peaks mainly originate from the Nb-d orbitals.

When the Nb content is increased to 4.55%, the Ag-d orbital cusp shifts to -7 eV , the density of states value of the Ni-d orbital increases, the orbital overlap peaks become more pronounced, and the hybridization is more intense; as illustrated in Figure 2c, within the $-7\text{ eV}\sim -3\text{ eV}$, the wave peaks mainly originate from the Ag-d orbitals, Ni-d orbitals, Nb-d orbitals, and Nb-s orbitals. In the region of $-3\text{ eV}\sim 20\text{ eV}$, the wave peaks mainly originate from the Ni-d and Nb-d orbitals.

Figure 2d illustrates the density of states of the Nb-doped(6.77) AgNi interface model. With the further increase in Nb content, the density of states of the Ni-d orbitals decreases, leading to a reduction in the number of electrons at the Fermi energy level. At $-6\text{ eV}\sim -3\text{ eV}$, the Ag-d orbitals, Ni-d orbitals, and Nb-d orbitals undergo hybrid coupling, forming bonded orbitals. The main source of the wave peaks does not change significantly.

3.3. Interface Bonding Characterization

The density of states diagram can determine the distribution of electrons in atomic orbitals and bonding. However, it is challenging to quantitatively describe the strength of bonding. Therefore, it is necessary to analyze the charge population and bond population to quantitatively determine the strength of bonding. This analysis should be combined with the results for the density of states to carry out an analysis of the interface bonding strength of the micro-mechanism. The Mulliken charge population is used to characterize the electron transfer between atoms. Atoms that are prone to losing electrons have a positive charge population, while atoms that are prone to gaining electrons have a negative charge population [22]. The larger the absolute value of the charge population, the stronger the ability to gain and lose electrons, and the higher the interfacial bonding strength. Table 5 displays the average charge population of the doped AgNi interfacial model obtained through simulation.

Table 5. Mulliken charge population.

Doping Ratio	Mulliken Charge Population		
	Ag	Ni	Nb
AgNi	-0.0040	0.0141	
AgNi-Nb(2.29)	-0.0052	0.0146	0.1100
AgNi-Nb(4.55)	-0.0061	0.0218	0.1800
AgNi-Nb(6.77)	-0.0044	0.0130	0.1200

Doping ratios in the table are all wt.%.

Table 5 shows that doping the AgNi interface model with varying amounts of Nb affects the electron gain and loss capabilities of each atom. Nb atoms have a positive charge population, suggesting that they all lose electrons during the electron transfer process. The electron transfer phenomenon becomes more prominent after the AgNi is doped with Nb(4.55), enhancing the ability of the Ag and Ni atoms to gain and lose electrons. Additionally, the Nb atom demonstrates a higher charge population, indicating a stronger ability to gain and lose electrons during the electron transfer process. Nb(2.29)-doped AgNi, Ag, and Ni atoms experience enhanced electron capacity changes, although the effect is

less pronounced compared to Nb(4.55) doping. With Nb(6.77) doping, Ag atoms exhibit increased electron capacity, while Ni atoms show a decrease in electron capacity.

The bond population is used to characterize the nature of interatomic bonding. The larger the absolute value of the bond population, the more the electron clouds overlap with each other, resulting in a stronger bonding ability and a more stable chemical bond being formed [23]. Table 6 shows the range of the bond population corresponding to each valence bond in the AgNi interfacial model before and after doping, as well as the average values obtained through simulation. If the value of the bond population is close to 0, a bond may be formed and it will be strongly ionic. The further the value of the bond population from 0, the more likely the valence bond is to be covalent. If the value of the bond population is less than 0, it is considered an anti-bond.

Table 6. Bond population.

Doping Ratio	Bond Population	
	Ag-Ni	Ni-Nb
AgNi	0.12~0.41/0.27	
AgNi-Nb(2.29)	0.22~0.38/0.33	−0.11~−0.36/0.24
AgNi-Nb(4.55)	0.24~0.43/0.38	−0.14~−0.50/0.31
AgNi-Nb(6.77)	0.04~0.38/0.31	−0.26~−0.46/0.15

Doping ratios in the table are all wt.%.

As can be seen from Table 6, the Ag-Ni bonds in the AgNi interfacial model all have positive values, indicating a certain degree of covalency. At room temperature, AgNi is a binary system where Ag and Ni are nearly immiscible. At the electronic structure level, there may be chemical bonds with some degree of covalency between the Ag and Ni atoms at the AgNi phase interface. At the atomic scale, the formation of Ag-Ni bonds in specific phase interface regions of the AgNi system is feasible. After doping, a specific bond fabric residence exists between atoms in all interfacial regions, which is consistent with the analysis of the interfacial bond strength and the density of states. After doping, the dopant atoms exhibited both bonding and antibonding states with Ni, influencing the overall bonding state. The strength of the Ag-Ni bonding in the Nb(4.55)-doped AgNi interfacial model is the highest, followed by Nb(2.29), and the lowest is Nb(6.77). Therefore, Nb doping can effectively enhance the AgNi interfacial stability by promoting the formation of more covalent bonds between Ni and Ag atoms. However, the AgNi interfacial stability shows a decreasing trend with a further increase in Nb content, although it remains superior to the undoped model.

The simulations predicted the best interfacial bond strength and the highest interfacial stability for Nb(4.55)-doped AgNi, which corresponds to the optimal wetting and electrical contact properties.

4. Experiment

4.1. Preparation of Ag/Ni Contact Materials

For AgNi materials, as the Ni content increases, higher temperatures and longer times are required to dissolve the original Ni particles in the Ag matrix. During condensation, it is easy to form a Ni-enriched area and some Ni oxide on the contact's surface. Therefore, an increase in Ni content will result in a significantly faster rise in the material's contact resistance. Even at a high temperature of 2000 °C, the solubility of Ni in Ag is only about 10%. When the nickel content in the material exceeds 10%, it becomes challenging for the "dissolution precipitation effect" to fully encapsulate all the original Ni particles [24]. In this case, the formation of Ni-enriched zones and the generation of oxides are inevitable, leading to a sharp increase in contact resistance. When the Ni content exceeds 20%, the above situation almost inevitably occurs. Therefore, the preparation of an undoped AgNi contact material with a 15% Ni content was chosen, and Ni powder of equal quality was used to replace the Nb powder for doping.

In this paper, AgNi contact materials were prepared by combining the high-energy ball milling method and powder metallurgy method. The prepared AgNi contact materials weighed 10 g. The atomic ratio of the additives to the mass ratio is shown in Table 1. The specific preparation process is as follows:

The powders were mixed in a high-energy ball mill by first thoroughly mixing half of the Ag powder with the Ni powder. Then, the Nb powder was added to the mixed powder and was homogeneously mixed with the remaining Ag powder again using high-energy ball milling. All of the aforementioned steps necessitated adding a corresponding amount of powder to the agate ball milling bottle, followed by the addition of agate balls, with the ball-to-powder ratio set at 50:1. Agate balls were selected as the grinding material to prevent impurities during the ball milling and mixing process, thereby enhancing the purity of the samples. Then, 3 mL of ethanol was added to the ball milling jar as a grinding medium to enhance the comminution efficiency. This addition helps refine the powder particles and prevent oxidation of the powder. The speed was set at 200 rpm and 500 rpm, and the ball milling time was 1 h. The ball milling jars were rotated 360° for multidimensional and multidirectional movement.

After drying, the composite powder was poured into a 20 mm diameter die and pressed into flakes. An initial pressure setting of 15 MPa and a holding time of 10 min resulted in a coin-shaped flake sample. After the initial pressing, the flake sample appeared to be solid, but the structure was still relatively loose and not dense enough when the powder was compacted solely by mechanical force. Through the sintering process, the internal bonding of the sample can be further enhanced, thus improving the mechanical strength of the material, increasing densification, and reducing internal porosity. The sintering process was carried out in a vacuum atmosphere at a temperature of 700 °C with a holding time of 90 min. The temperature was then gradually reduced to 300 °C at a rate of 10 °C per minute and cooled to room temperature naturally. Further re-pressing and re-firing were required to increase the overall density of the material. The pressure was set at 20 MPa, and the holding time was 10 min. The re-pressurized sample was burned to reduce the particle spacing and increase the level of densification. The process was carried out in a vacuum atmosphere at 650 °C for 90 min. The samples were then cooled to 300 °C and allowed to naturally cool to room temperature before being removed. Finally, grinding and polishing were carried out. Fine water-abrasive paper was moistened and suctioned flat onto an abrasive disc. The sample embryo was held on the sandpaper, ensuring that it was directly below the head hole. Grinding was then started. The grinding parameters were set as follows: grinding time of 2 min, pressure of 20 N, and speed of 90 rpm. After grinding, the surface of the sample appeared bright and flat, but minor scratches were still visible to the naked eye. For this reason, a polishing process was used to reduce the scratches and improve the surface finish of the sample. A tweed polishing disc was placed flat in the polishing operation position, and the material was then placed on this disc. The polishing operation involved spraying the polishing compound every 5 s. The polishing parameters were set as follows: polishing time of 2.5 min, pressure of 20 N, speed of 150 rpm.

The sheet obtained after the aforementioned steps was processed by wire cutting to produce an AgNi electrical contact with a diameter of 3.2 mm and a length of 3.3 mm. The preparation process flow depicted above is shown in Figure 3.

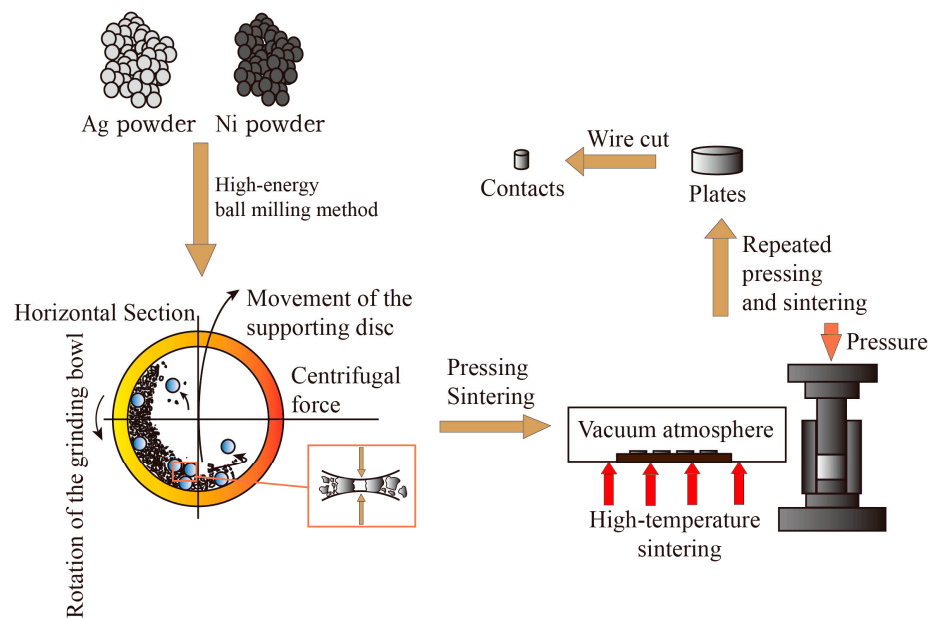


Figure 3. Process flow for the preparation.

4.2. Preparation of Ag/Ni Contact Materials

The droplet morphology on the solid surface is shown in Figure 4. θ denotes the wetting angle between the liquid–gas interface and the solid–liquid interface. In other words, the tangent line to the liquid–gas interface is drawn over the contact point of the solid–liquid–gas interface, and the angle between this tangent line and the solid–liquid interface.

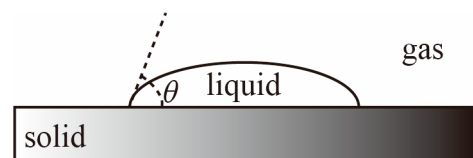


Figure 4. Droplet morphology and wetting angle on solid surfaces.

The wetting angle $\theta = 0^\circ$ indicates that the liquid can completely spread on the solid surface, forming a liquid film, showing complete wettability of the liquid on the solid surface. A wetting angle within the range of $0^\circ < \theta < 90^\circ$ indicates that droplets on the solid surface can partially spread, forming a relatively flat droplet, and the droplets can partially wet the solid surface, demonstrating good interfacial stability between the two phases. A wetting angle within the range of $90^\circ < \theta < 180^\circ$ indicates that droplets on the solid surface almost do not spread at all, forming a highly protruding “sitting” droplet, with weak interfacial bonding stability [25]. The wetting angle is between 90° and 180° , indicating that the droplet almost does not spread on the solid surface, forming a highly protruding “sitting” droplet, and the interfacial bonding stability is weak.

The detailed procedure for wetting angle measurement is as follows: Firstly, Ag, Ni, and Nb powders were weighed quantitatively. The total mass of the substrate material was 3 g. If the undoped Ni phase was used as the substrate, 3 g of Ni powder was weighed. If the Nb-containing Ni phase was used as the substrate, 2.7 g of Ni powder and 0.3 g of Nb powder were weighed. Additionally, 0.3 g of Ag powder was weighed. Subsequently, the weighed substrate powder material was placed into the planetary ball mill for mixing. Onyx balls were used as the ball material, and anhydrous ethanol was added to the grinding jar. After drying, the substrate material was pressed into a sheet. Since the total mass of the powder was only 3 g, a pressure of 5 MPa was applied to prevent the substrate from cracking, and the holding time was set to 5 min. Subsequently, the pressed Ni phase substrate was placed in a vacuum tube furnace for sintering. The temperature was set

to 1100 °C, and the holding time was set to 5 min. The sintering temperature was set at 1100 °C, and the holding time was set to 60 min. Afterwards, Ag powder was uniformly placed on the Ni plate and sintered. This process caused the Ag powder to melt into molten droplets, ensuring that it could naturally spread on the Ni phase substrate. The melting point of Ag was 961.93 °C. To ensure complete melting, the sintering furnace temperature was set to 1050 °C, and the holding time was set to 30 min. Afterwards, the wettability angle was measured, and the images were captured by a computer to determine the wetting angle of the Ag powder. A computer was used to intercept the images and measure the wetting angle on both sides.

Figure 5a–d show the wetting angle measurements of AgNi contact materials before and after doping, respectively. As can be seen from Figure 5, after doping, the diffusion between Ag and the substrate is enhanced, the penetration is evident, and the wettability is improved. The wetting angle of AgNi before and after doping is less than 90°. The wetting angle of undoped AgNi contact material is close to 90°, indicating poor wettability between Ag and Ni. After doping, the wetting angles are reduced. The wetting angle of Nb(4.55)-doped AgNi contact material is the smallest, followed by the wetting angle of Nb(2.29)-doped AgNi contact material, and finally the wetting angle of Nb(6.77). The wettability ranking aligns with the ranking of interfacial bond strength.

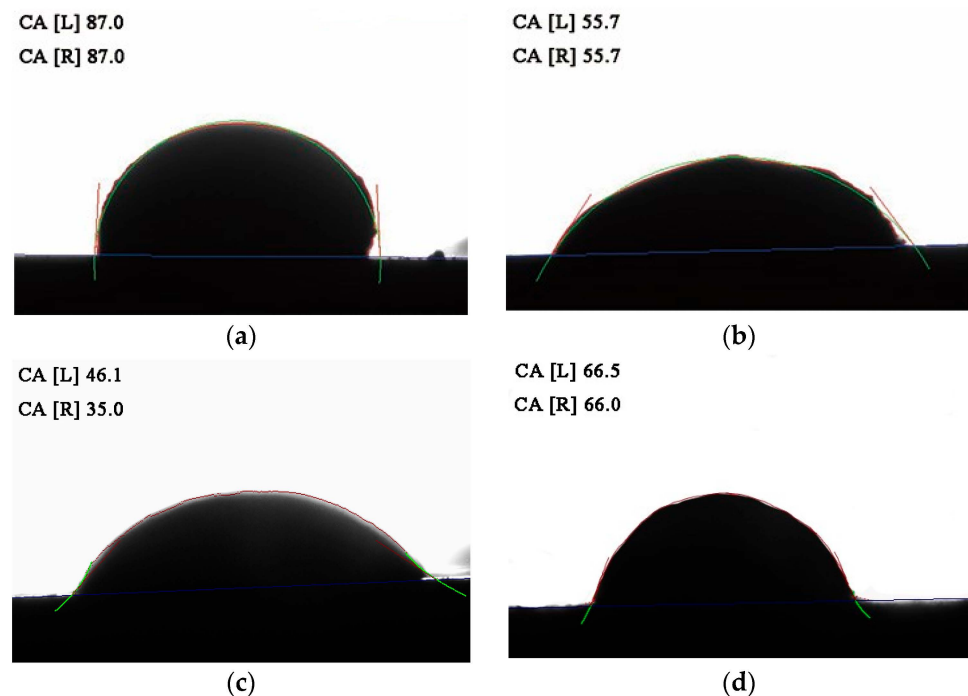


Figure 5. Wetting angle of Nb-doped contact materials: (a) AgNi, (b) AgNi-Nb(2.29), (c) AgNi-Nb(4.55), and (d) AgNi-Nb(6.77).

4.3. Electrical Contact Experiments

In this paper, the JF04D electrical contact material performance test system was utilized to conduct electrical contact simulation experiments, enabling direct measurement of the electrical contact parameters of each contact. A schematic diagram of the JF04D electrical contact material test system is illustrated in Figure 6. The test system's start-up protection voltage was set at ± 40 V, with a DC voltage of 24 V, an experimental current of 15 A, an operational frequency between the contacts of 60 times per minute, and a contact pressure set at 86 cN. Due to the experimental use of DC voltage and current, the AC arc "zero rest" phenomenon is absent. This absence leads to more serious contact erosion. Additionally, the JF04D electrical contact material test system does not have an arc-extinguishing device. Therefore, considering these factors, the number of electrical contacts was set at 10,000 times, with an average value being taken every 100 times as one data point. The

JF04D electrical contact material testing system did not have an arc-extinguishing device installed. Therefore, with the electric contact frequency set at 10,000 times, the average value for each cycle was established with 100 times being one data point. Electrical contact performance testing involves using a test stand to simulate the separation action of the moving and static contacts multiple times to replicate the process of disconnecting and closing actions. At the moment of separation, a high-temperature arc is generated. At this point, the energy of the arc near the anode of the moving contact is higher than the energy of the arc near the cathode of the static contact. The ablation effect of the arc at the anode of the moving contact is more severe. Therefore, Nb-doped AgNi anode contact material was mounted on the dynamic contact, and undoped AgNi cathode contact material was mounted on the static contact to observe the impact of varying levels of Nb doping on the arc erosion resistance of the AgNi electrical contact material.

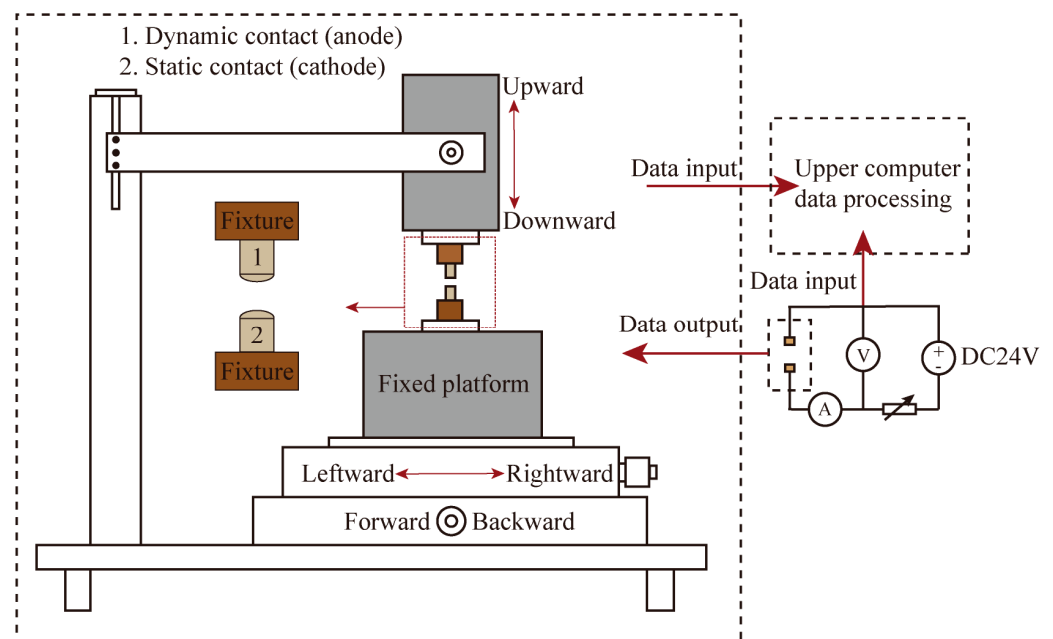


Figure 6. JF04D electrical contact material testing system.

Arc energy, arc duration, and welding force are important parameters for assessing the performance of contact materials [26]. During the electrical contact performance test process, the contact material experiences a gradual decrease in dynamic and static contact pressure upon separation. Consequently, the actual contact surface between the contacts diminishes, leading to an increase in current density at the contact point. This increase results in a rapid temperature rise, potentially reaching the melting point of the metal or even the boiling point of the contacts. This can generate an arc between the contacts, causing arc erosion, material transfer, and other physical and chemical processes in the electrical contact material [27]. An arc is a physical phenomenon due to electrical contact during performance experiments. The degree of arc erosion becomes more serious with the increase in arc energy, while the arc energy increases with the lengthening of the arc duration. During the repetitive breaking and closing process of the electric contact surface, a high-temperature arc is generated, leading to localized melting. The severity of the contact is determined by the stability of the welding after the melting of the contact. The force required to separate the welding contact at its smallest breaking point is referred to as the fusion welding force. When the breaking force is less than the fusion welding force, the contact cannot undergo normal breaking, contact welding, or electrical function failure, resulting in a smaller electrical contact welding force being considered better for anti-melting welding performance with the contact material. Figures 7–9 display the

relationship curves between arc ignition energy, arc ignition time, welding force, and the number of operations with varying Nb doping contents, respectively.

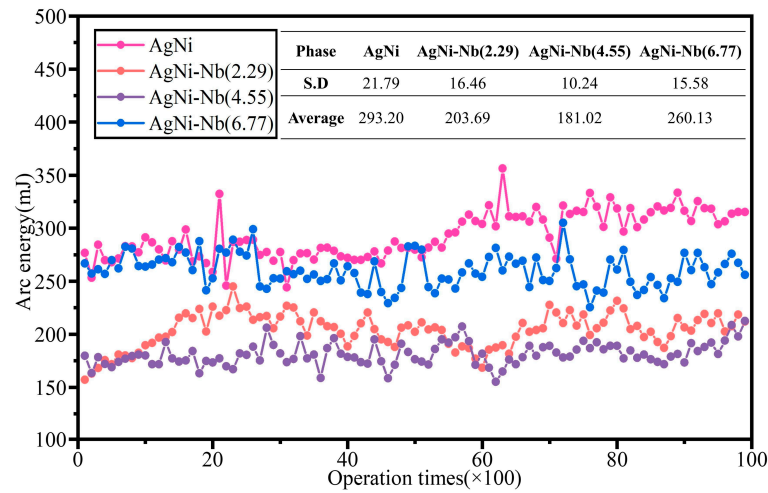


Figure 7. Curve of arc energy versus number of operations.

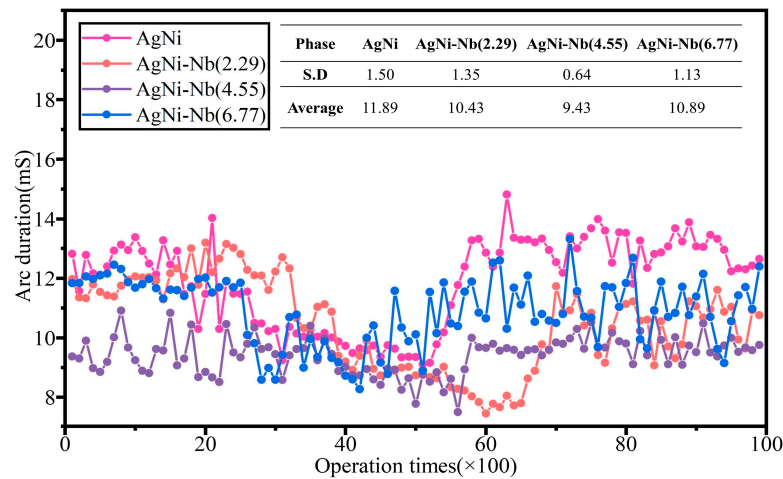


Figure 8. Curve of arc duration versus number of operations.

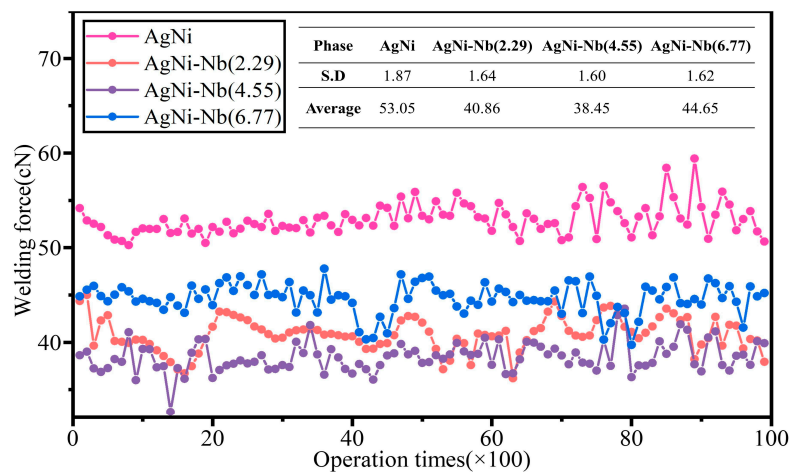


Figure 9. Curve of welding force versus number of operations.

As shown in Figure 7, doping with Nb effectively reduces the arc energy of AgNi contact materials. With an increase in Nb content, the average arc energy of the electrical

contact materials decreased by 30.53%, 38.26%, and 11.28%, respectively. This enhancement improves stability, and the distribution of waveform curves ranges from 150 mJ to 310 mJ. The arc energy does not show a significant increase with the increase in the number of passes when doped with Nb. The degree of improvement in performance with the increase in Nb content showed a trend of initially increasing and then decreasing. Among them, the Nb(4.55)-doped arc energy decreased significantly, while the Nb(6.77)-doped arc energy showed a significant difference with the undoped material after only about 5000 passes. In addition, after Nb(4.55) doping, the arc energy decreased significantly after about 5700 cycles, indicating that with the increase in the number of operations, the high temperature generated by the arc leads to the melting of the contact surface of the fine burrs. The surface smoothness was slightly improved, and the arc energy then declined. With Nb(6.77) doping, until about 7200 cycles, the arc energy did not show a significant downward trend. By 7500 cycles, the arc energy had continued to rise. The number continued to rise to around 7500 times. The above phenomenon demonstrates that, with the further increase in Nb content, the decrease in the basal elements, especially Ni content, weakened the dissolution–precipitation effect. This led to the formation of many Nb-Ni alloys and other precipitates, further diminishing the impact of the dissolution–precipitation effect. Simultaneously, it resulted in material inhomogeneity, intensified arcing, and serious erosion of the surface morphology.

Arc duration is the time from the start of combustion to extinguishment, and it is correlated with arc energy. Generally, a higher arc energy results in longer arc durations and more pronounced erosion effects on the contact surface. Figure 8 shows that the impact of varying Nb doping content on arc duration is similar to its effect on arc energy. However, the changes in arc duration are more pronounced than those in arc energy. Specifically, Nb(2.29) doping results in a slight delay in the decline and subsequent rise in arc duration compared to other doping materials.

As can be seen from Figure 9, with the increase in Nb content, the fusion welding force shows a tendency to decrease first and then increase, but the improvement in stability is not significant. Under the high-temperature arc, the temperature of the arc root area increases instantly. Ni particles are rapidly dissolved in the Ag droplets in the molten state. As the arc extinguishes, the temperature decreases, causing the Ni dissolved in the Ag solution to precipitate. This process easily forms an enriched area on the contact surface, leading to a sharp rise in contact temperature. Consequently, the metal melting pool expands, resulting in an increased actual fusion welding area, thereby enhancing the fusion welding force [28]. During the experimental process, the material between the AgNi contacts is transferred due to the arc's action, leading to variations in contact pressure on the contact surface. These variations subsequently influence the fusion welding force. Nb can be utilized to achieve a uniform distribution of precipitates by promoting precipitation and regulating the cooling rate. This approach can also manage the arc in specific local areas where it initiates ignition, enhancing the resistance to melting and welding. Excessive amounts of Nb can enhance the strengthening effect of material grain boundaries, hindering their movement and deformation. This, in turn, increases the resistance to deformation and thermal deformation during fusion welding, ultimately requiring a higher fusion welding force.

In addition, by comparing similar research papers, we found that the arc energy of undoped AgNi(10) electrical contact materials prepared by the high-energy ball milling method decreased by 60.9% compared to the conventional mixing method [29]. The arc energy of AgNi doped with 2.29% and 4.55% Nb decreased by 2.5% and 13.4%, respectively, compared to the same material doped with 1.38% Cu. In contrast, the arc ignition energy of the material doped with 6.77% Nb increased by 24.4%. The melting force of AgNi contact materials with three different levels of Nb doping decreased by 44.4%, 47.6%, and 39.2%, respectively, compared to 1.38% Cu doping [30]. The superiority of Nb-doped AgNi contact material has thus been proven.

In summary, the analysis of AgNi electrical contact materials regarding arc energy, arc duration, and welding force indicates that Nb doping can effectively enhance the degree of arc erosion of AgNi electrical contact materials and the degree of material transfer. As the Nb content increases, the degree of arc erosion of the contact initially decreases and then increases, aligning with the simulation results.

5. Contact Arc Erosion Morphology

5.1. 2D Macroscopic Arc Erosion Morphology

Dynamic and static contacts generate high-temperature arcs during multiple electrical contacts. The contact surfaces of the contacts undergo metal melting, droplet spattering, surface spalling, and other phenomena under the ablation of the arc, resulting in changes in the surface morphology of the AgNi contact material.

Figure 10 shows the scanning electron microscope (SEM) surface morphology of the anodes and cathodes of AgNi electrical contact materials with varying Nb content doping. The undoped AgNi contact exhibits severe surface ablation on the anode, characterized by numerous erosion pits distributed across the entire surface, while the cathode displays a hill-like bulge. When Nb(2.29) is doped, the number of erosion pits on the anode is greatly reduced. In some areas, there is no obvious erosion morphology, but there are a small number of mound-like protrusions and Ag melt flow traces on the cathode. Additionally, a small number of erosion pits appear in the center of the cathode. When Nb(4.55) is used for doping, the number, area, and depth of erosion pits are further reduced. The area affected by Ag melt flow only represents about two-thirds of the contact surface area. The cathode erosion pits completely disappear, with only a slight elevation remaining. This indicates that the degree of arc erosion of the contact material decreases as the Nb content increases. When the Nb content increases to 6.77%, the Ag melt flow area is distributed across almost the entire contact surface. The number and depth of erosion pits exceed those when Nb(4.55) is used, leading to an increased degree of cathode surface bulge and deeper material transfer. At the same doping content, the surface erosion on the anode is more severe than that on the cathode. Moreover, as the doping content increases, the morphological changes on the anode surface become more pronounced compared to those on the cathode. This suggests that the arc erosion resulting from the higher Nb content has a more significant effect on the anode.

5.2. 3D Macroscopic Arc Erosion Morphology

The 2D macroscopic morphology of the contact can effectively demonstrate the degree of arc erosion in the X and Y directions and visually indicate the size of the eroded area. However, SEM pictures cannot capture detailed information about the surface profile of AgNi contact materials. In this paper, the 3D macro-arc erosion morphology of AgNi electrical contact material surfaces under different Nb doping contents was collected and constructed using an OLYMPUS-DSX 1000 3D microscope. The equipment was provided by Olympus Corporation in Shenzhen, China. In order to more intuitively illustrate the erosion of the contact surface, this paper only visualizes the surface above 1.7 mm for the anode and 2.8 mm for the cathode, and obtains the three-dimensional morphology of the AgNi contact surface as depicted in Figure 11.

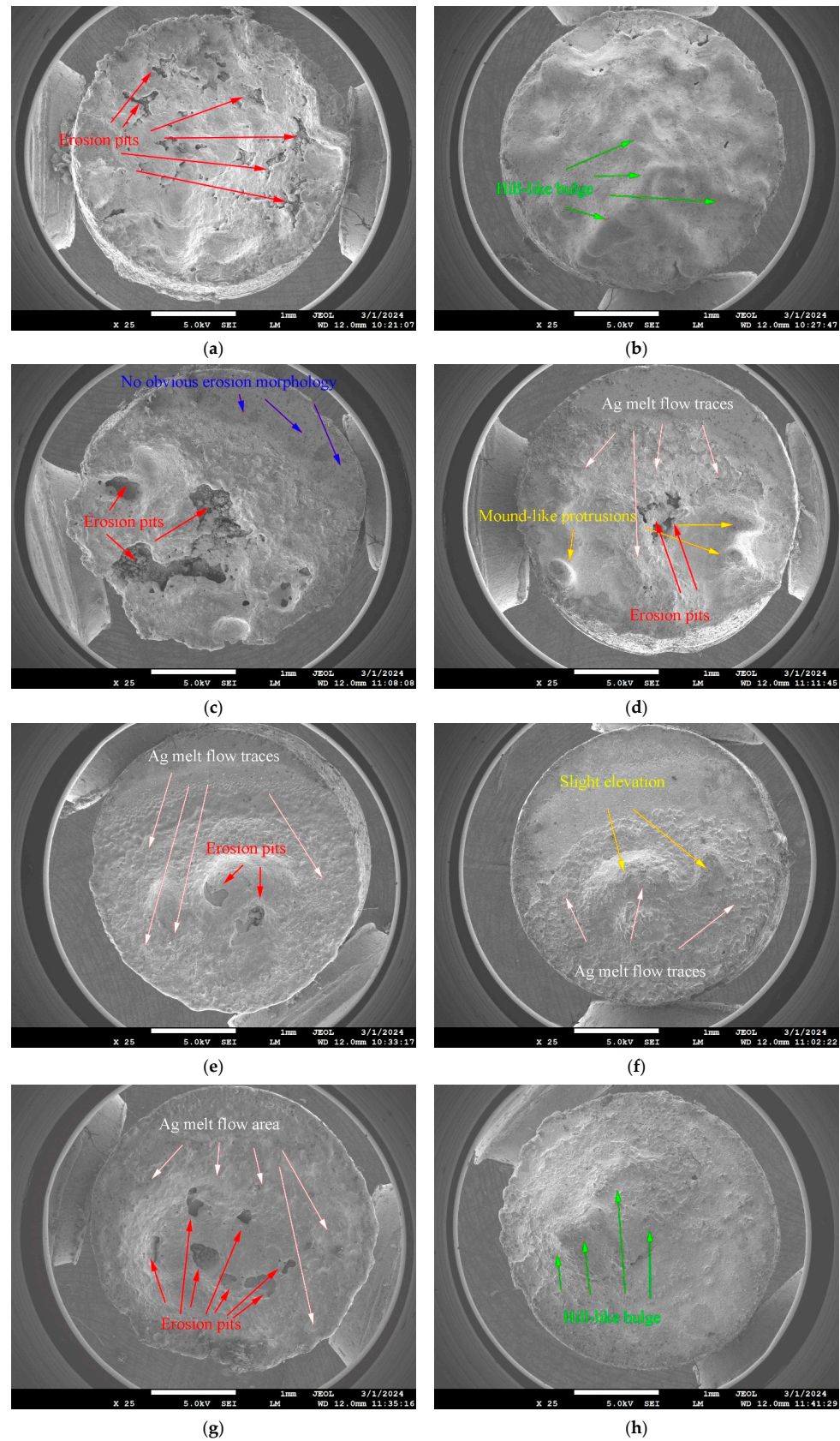


Figure 10. Two-dimensional morphology of AgNi contact surface with different amounts of Nb doping: (a) AgNi anode, (b) AgNi cathode, (c) AgNi-Nb(2.29) anode, (d) AgNi-Nb(2.29) cathode, (e) AgNi-Nb(4.55) anode, (f) AgNi-Nb(4.55) cathode, (g) AgNi-Nb(6.77) cathode, and (h) AgNi-Nb(6.77) anode.

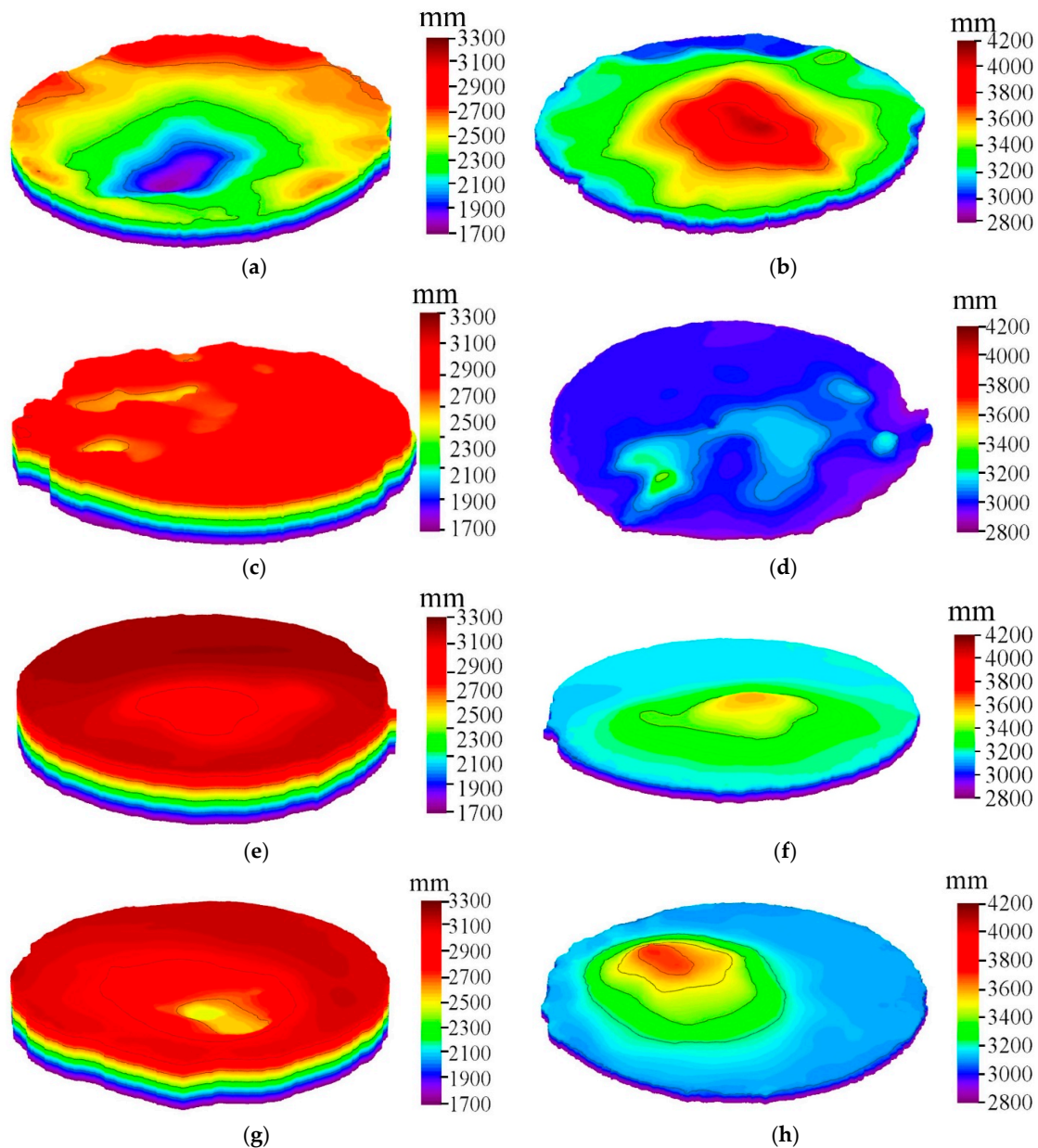


Figure 11. Three-dimensional morphology of AgNi contact surface with different contents of Nb doping: (a) AgNi anode, (b) AgNi cathode, (c) AgNi-Nb(2.29) anode, (d) AgNi-Nb(2.29) cathode, (e) AgNi-Nb(4.55) anode, (f) AgNi-Nb(4.55) cathode, (g) AgNi-Nb(6.77) cathode, and (h) AgNi-Nb(6.77) anode.

With the increase in Nb content, the 3D morphology of the AgNi contact surface showed varying degrees of changes. Pits appeared on the anode and peaks appeared on the cathode. The number of pits and the height of peaks seemed to decrease and then increase with the increase in Nb content. This suggests that the material transfer direction was from the anode to the cathode. The Nb content initially reduced and then intensified the erosion of the arc on the AgNi electrical contacts.

With undoped Nb, a large erosion pit with a depth of 1.6 mm appeared on the anode contact. In contrast, the anode contact, after doping with 2.29% Nb, exhibited several erosion pits with a smaller area and a significantly reduced depth of about 0.8 mm compared to the undoped state. When the Nb content was increased to 4.55%, the dense erosion pits had disappeared, and the surface of the anode contact appeared to have a shallow depth of about 0.4 mm. When the Nb content is increased to 6.77%, the erosion pit

becomes deeper, reaching a depth of 0.9 mm. This depth is rougher than the erosion pit shown in Figure 11e and will lead to increased erosion of the contacts by the arc.

Under the same doping conditions, the trend of cathode surface changes is essentially similar to that of the anode. However, the 3D macroscopic morphology changes on the anode are more severe than those on the cathode. Combined with the two-dimensional morphology of the anode and cathode, it can be concluded that under the same doping conditions, the anode is more sensitive to arc erosion than the cathode. The effect of different Nb doping content on the anode is more pronounced than on the cathode, and the degree of arc erosion on the surface shows a decreasing and then increasing trend with the increase in Nb content.

5.3. Characteristics of Microscopic Arc Erosion Morphology

Under different Nb content doping, the arc action resulted in various micro-erosion features on the contact surface. As can be seen in Figure 12, the arc erosion morphology on the surfaces of the cathode and anode’s electrical contacts varies with different Nb contents. Additionally, the surface morphology characteristics of the cathode and anode contacts differed even with the same Nb content doping.

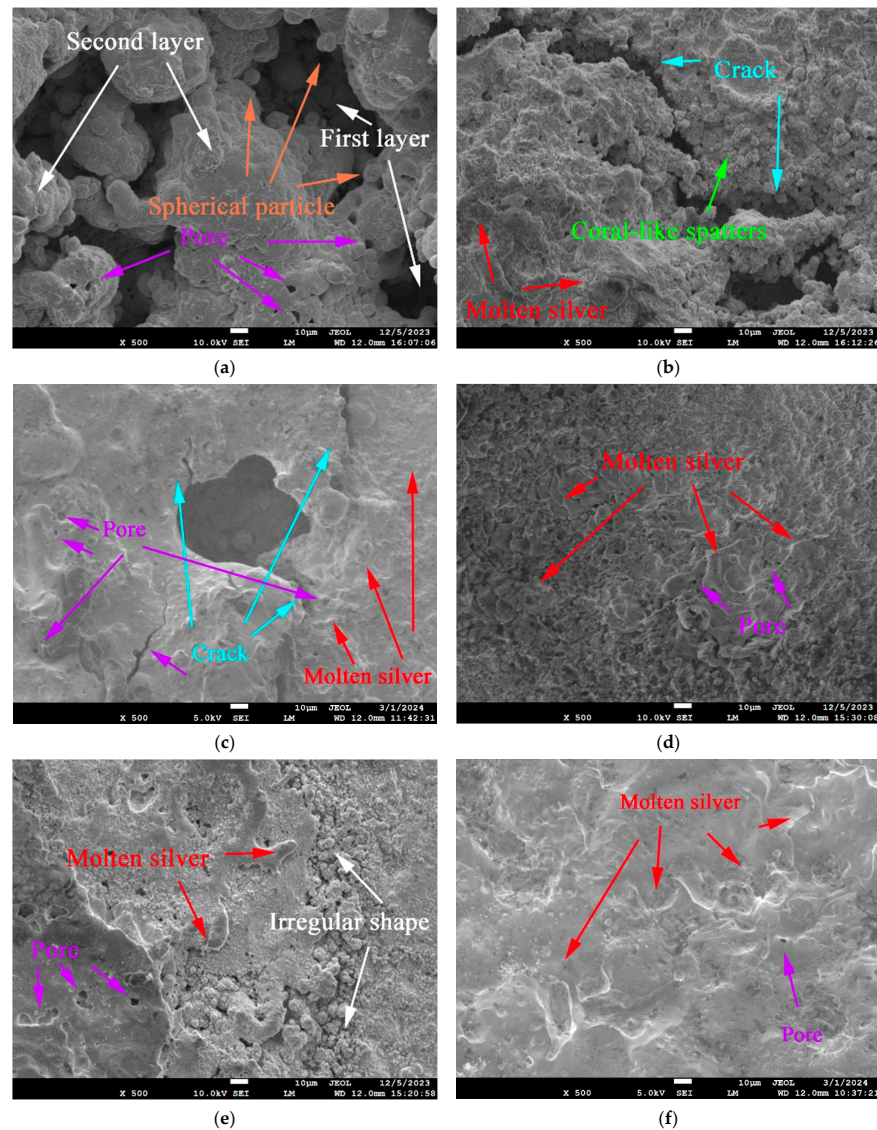


Figure 12. Cont.

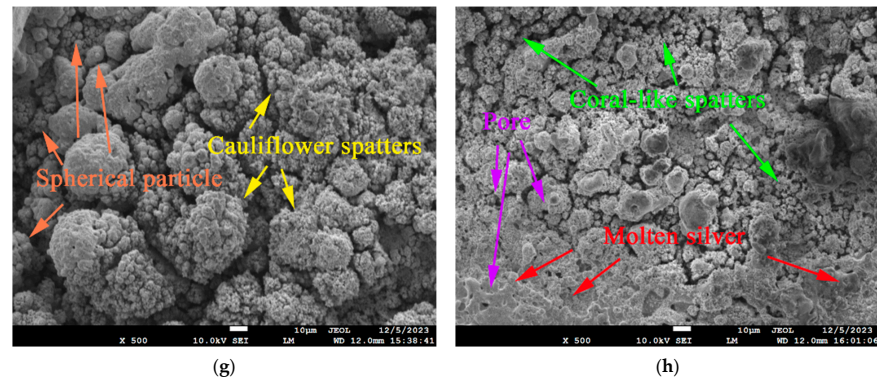


Figure 12. Surface microscopic morphology of AgNi contacts with different contents of Nb doping: (a) AgNi anode, (b) AgNi cathode, (c) AgNi-Nb(2.29) anode, (d) AgNi-Nb(2.29) cathode, (e) AgNi-Nb(4.55) anode, (f) AgNi-Nb(4.55) cathode, (g) AgNi-Nb(6.77) cathode, and (h) AgNi-Nb(6.77) anode.

On the undoped AgNi contact material anode surface, numerous holes were observed, mostly in close-to-spherical shapes. Additionally, a clear layering of spatter erosion products was evident. The cathode surface exhibited wider cracks. With an Nb doping content of 2.29%, the anode surface of the contact still showed remnants of molten silver traces. The number and size of holes decreased, and the distribution of erosion pits around the cracks also decreased. When the Nb doping content was 4.55%, the anode contact surface showed a small amount of molten Ag traces, irregularly shaped spatters, and some pores, while the cathode surface was smoother than that doped with Nb(2.29), and the pore phenomenon almost disappeared. When the Nb doping content reached 6.77%, the molten Ag on the anode surface basically disappeared. Instead, a dense cauliflower-like morphology with various sizes of spherical spatter particles emerged. Some molten Ag was still present on the cathode surface, and there was no significant alteration in the density and size of the pore distribution. However, some coral-like structures of spatters were observed.

Due to the solubility of oxygen in liquid silver (0.3%) being 40 times higher than in solid silver (0.008%), molten silver absorbs oxygen from the air when exposed to an arc. When the contact is broken, a change in oxygen pressure causes some of the dissolved oxygen in the molten silver to escape into the air, while another portion of the oxygen, due to the rapid solidification of the molten silver, does not escape in time. This leads to the formation of holes on the surface and inside the contact, affecting the performance of the AgNi contact material. During the electric contact experiment, when the contact break occurs and the arc extinguishes, the temperature drops suddenly. As a result, the surface of the molten layer undergoes rapid cooling and solidification. This rapid solidification causes an increase in the density of vacancies and dislocations within the molten layer's structure. Consequently, the strength of the grain boundaries decreases, leading to an increased likelihood of crack formation.

Nb can induce the uniform precipitation of Ni, which enhances the densification of the contact surface and reduces porosity, thereby facilitating arc extinguishing. When the Nb content is further increased, at the end of the ignition arc, the melt temperature drops rapidly, resulting in supercooling. This is dependent on the growth of the un-melted matrix, leading to a negative temperature gradient. Additionally, a large number of Nb-Ni precipitates form, creating a microstructure with a cauliflower-like morphology.

6. Mechanism of Nb Doping on Arc Erosion of Electrical Contact Materials

The flow in the molten pool influences the erosion pattern and material transfer of the electrical contact material. In a molten pool, when an electric current passes through the molten pool, a magnetic field is generated around the current. This magnetic field interacts with the current, resulting in the Lorentz force, which affects the liquid metal in the molten pool. As illustrated in Figure 13, the Lorentz force induces a change in the flow direction of

the molten pool as the current passes through it. This results in the molten pool moving downward from the center and then upward along the walls. The Lorentz force caused by the current results in the anode melt pool flowing in the cathode direction, while the cathode melt pool flows in the opposite direction. This phenomenon makes the spattering of the anode more pronounced, and the erosion morphology of the cathode surface is characterized by the flow traces of the Ag melt. The high melting point of Nb, improved wettability after doping, and lower arc-firing energy enhanced the viscosity of the melted Ag, reducing droplet splashing and weakening the flow in the melt pool. Consequently, the surface of the AgNi contact became flatter.

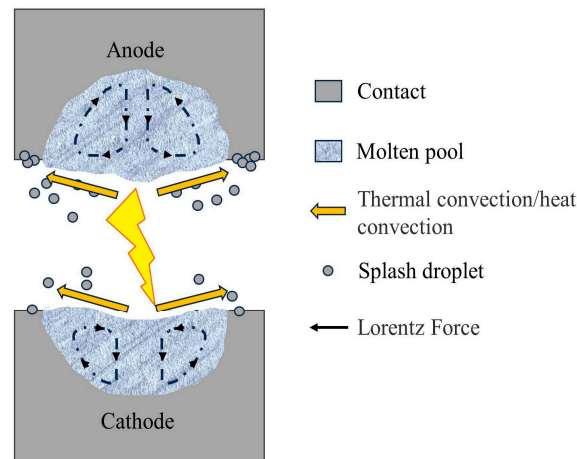


Figure 13. Physical modelling of AgNi contact molten pool.

In addition, Nb can form stable carbides and nitrides with Ni in the matrix. These precipitates are generated at grain boundaries, effectively hindering the slip and diffusion of grain boundaries. This process increases the toughness and strength of grain boundaries. The precipitates at the grain boundaries can also create dislocation shielding effects, which prevent the propagation of dislocations and consequently enhance the fatigue resistance of the material. The operation of the grain boundary strengthening mechanism enables Nb-Ni alloys to exhibit excellent thermal creep and fatigue resistance in high-temperature environments. These alloys can withstand prolonged exposure to high temperatures without undergoing plastic deformation or fracturing easily. By adding an appropriate amount of Nb in the solid solution state, the matrix grains can be effectively refined, and the formation of precipitated phases can be promoted. This grain refinement can hinder the movement and slip of dislocations, increasing the strength and hardness of the material. The addition of Nb can also reduce the energy of the grain boundary of the alloy, improving the stability of the grain boundary. This further enhances the hardness and toughness of the grain boundary region and affects the thermal creep behavior of the alloy, making it more stable and reliable at high temperatures.

7. Conclusions

In this paper, based on the first principle, an interfacial model of AgNi doped with varying amounts of Nb was simulated and tested to analyze the interfacial stability and bonding strength and predict the wettability. After that, AgNi electrical contact materials with different Nb doping levels were prepared by combining powder metallurgy and high-energy ball milling. Subsequently, 10,000 electrical contact tests were conducted on the materials to analyze the arc energy, arc duration, and welding force. The 2D macro- and microscopic morphologies of the post-test contacts were analyzed using SEM, while the 3D macro-morphology was constructed and analyzed by a 3D morphology instrument. Additionally, a contact molten pool model was constructed to analyze the mechanism of

Nb doping affecting the arc erosion behavior of AgNi electrical contact materials. The following conclusions were obtained:

- (1) The interfacial separation work and interfacial energy of AgNi, as well as various Nb doping levels, are positive. They all contribute to forming a stable interface after doping, enhancing the interfacial stability of AgNi. Ag-Ni bonds may form in the interfacial region of the AgNi phase at the atomic scale. The simulation results suggest that Nb(4.55)-doped AgNi contact materials exhibit the best wettability and electrical contact properties.
- (2) The Nb doping content significantly affects arc formation and interruption, consequently influencing the electrical properties of AgNi electrical contact materials. Under different doping levels, the arc energy and arc duration curves of AgNi electrical contact materials exhibit a similar trend. With the increase in Nb doping content, the average and standard deviation of the arc energy, arc duration, and welding force show a pattern of initially decreasing and then increasing. This pattern confirms the accuracy of the simulation results. Under the action of an electric arc, the surface morphology of AgNi electrical contacts changes as the Nb content increases, following a trend that is essentially consistent with the results of electric contact experiments. Under the same conditions, the degree of ablation of the anode contact is more severe than that of the cathode, and the anode is more sensitive to changes in Nb doping content than the cathode.
- (3) The Lorentz force acting on the liquid metal in the molten pool due to the current results in spattering on the anode and silver melt flow traces on the cathode. The inclusion of niobium enhances the viscosity of the molten pool and diminishes droplet spattering. At the same time, the grain-boundary-strengthening and solid-solution-strengthening mechanisms of niobium provide the contacts with improved high-temperature stability, strength, and heat resistance.

Author Contributions: Conceptualization, J.W.; methodology, M.W.; formal analysis, G.H.; investigation, J.C.; resources, J.W.; writing—original draft preparation, M.W.; writing—review and editing, M.W.; project administration, J.W. All authors have read and agreed to the published version of the manuscript.

Funding: This research was funded by [S&T Program of Hebei] grant number [225676163].

Institutional Review Board Statement: Not applicable.

Informed Consent Statement: Not applicable.

Data Availability Statement: The data used to support the findings of this study are available from the corresponding author upon request.

Conflicts of Interest: Authors Jing Chen and Guanglin Huang was employed by the company Wenzhou Juxing Electric Contact Technology Co., Ltd. The remaining authors declare that the research was conducted in the absence of any commercial or financial relationships that could be construed as a potential conflict of interest.

References

1. Fu, R.; Liang, H.M.; Ye, X.R.; You, J.X.; Wei, Z. Analysis of the contact overtravel of contactor and its degradation state evaluation. *Trans. China Electrotech. Soc.* **2020**, *335*, 125–133. [[CrossRef](#)]
2. Li, H.Y.; Wang, X.H.; Xi, Y.; Zhu, T.; Guo, X.H. Effect of Ni addition on the arc-erosion behavior of AgTiB₂ contact material. *Vacuum* **2019**, *161*, 361–370. [[CrossRef](#)]
3. Kim, S.K. Process Development of Low-cost AgNi and AgFe Contact Materials with no Range of Solid Solubility. *Adv. Mater. Res.* **2008**, *47–50*, 873–876. [[CrossRef](#)]
4. Ling, G.P.; Xue, T.; Ni, M.L.; Liu, Y.T. Research on arc erosion products on silver-metal oxide contacts materials. *Precious Met.* **2008**, *29*, 1–5.
5. Wang, J.Q.; Hu, D.K.; Zhu, Y.C.; Guo, P.J. Electrical properties of In situ synthesized Ag-Graphene/Ni composites. *Materials* **2022**, *15*, 6423. [[CrossRef](#)] [[PubMed](#)]

6. Wang, Z.Y.; Liu, H.; Huang, X.W.; Zhang, T.J.; Li, B. Effects of Tungsten and Tungsten Oxide Particles on Contact Performance for Silver-Nickel Contacts. *Electr. Eng. Mater.* **2015**, *02*, 3–6+12. [[CrossRef](#)]
7. Li, A.K.; Zhou, W.Y.; Xie, M.; Wang, S.; Wang, S.B.; Yang, Y.C.; Chen, Y.T.; Liu, M.M. Preparation and arc erosion behavior of AgNi10 contact material with different allotropes of carbon addition. *Diam. Relat. Mater.* **2020**, *111*, 108141. [[CrossRef](#)]
8. Wang, J.Q.; Wang, M.H.; Zhang, Y.X. Simulation calculation and experimental study on the properties of Re, In, and Nb-doped Ag/Ni electrical contact materials. *IEEE Trans. Compon. Packag. Manuf. Technol.* **2024**, *14*, 619–629. [[CrossRef](#)]
9. Yang, C.L.; Zhang, X.F.; Yan, X.F.; Bai, X.P.; Zhang, M.J. Study on Silver Nickel Contact Material for High-Performance Relay. *Electr. Eng. Mater.* **2021**, *3*, 9–14. [[CrossRef](#)]
10. Li, S.H.; Yu, X.; Li, G.W.; Bai, X.P. Study on the Electrical Property of AgNi Contacts. *Electr. Eng. Mater.* **2011**, *02*, 7–12. [[CrossRef](#)]
11. Chen, J.-H.; Chen, S.; Xie, M.; Hu, J.-Q.; Wang, S.-B. High-speed imaging observation on molten bridges of AgNi10 electrical contact material. *Rare Metals* **2023**, *42*, 336–345. [[CrossRef](#)]
12. Ding, J.X.; Sun, Z.M.; Zhang, P.G.; Tian, W.B.; Zhang, Y.M. Current research status and outlook of Ag-based contact materials. *Mater. Rev.* **2018**, *32*, 58–66. [[CrossRef](#)]
13. Guo, T.F.; Fu, C.; Wang, J.B.; Liu, S.T.; Xue, Y.Y.; Zhao, H.G. Research and progress of silver-nickel contact materials containing additives. *Electr. Eng. Mater.* **2015**, *03*, 34–38. [[CrossRef](#)]
14. Xue, H.; Tong, X.H.; Song, Y.; Wang, F.; Liang, Y.F.; Peng, H.; Wang, Y.L.; Lin, J.P. Microstructure characteristics of a γ single-phase Ti-55Al-7.5Nb alloy fabricated via additive manufacturing. *Intermetallics* **2023**, *163*, 107984. [[CrossRef](#)]
15. Guan, W.M.; Pan, Y.; Zhang, K.H.; Guo, J.M. First principle study on the interface of Ag/Ni Composites. *Rare Met. Mater. Eng.* **2010**, *39*, 1339–1343. [[CrossRef](#)]
16. Zhao, Y.-R.; Zhang, H.-R.; Zhang, G.-T.; Wei, Q.; Yuan, Y.-Q. First-principles investigation on elastic and thermodynamic properties of Pnnm-CN under high pressure. *AIP Adv.* **2016**, *6*, 125040. [[CrossRef](#)] [[PubMed](#)]
17. Wang, X.; Du, X.M.; Li, J.D. First Principle Calculation of Stability of Ag/Ni Composites Interface. *J. Shenyang Ligong Univ.* **2023**, *42*, 55–60.
18. Zhang, Y.; Wang, J.Q.; Kang, H.L. Study on Electrical Properties of AgSnO₂ Contact Materials Doped with Rare-Earth La, Ce, and Y. *IEEE Trans. Compon. Packag. Manuf. Technol.* **2019**, *9*, 864–870. [[CrossRef](#)]
19. Liu, J.D.; Wang, X.; Du, X.M.; Xie, M.; Li, J.G.; Zhao, S.Q.; Zhou, Y.Z.; Zhang, Q.; Fang, J.H. Structural and elastic properties of AgNi10 alloy studied with ab-initio calculations. *Mater. Tehmol.* **2022**, *56*, 149. [[CrossRef](#)]
20. Cao, Y.X.; Wang, Y.H.; Li, H.; Chen, W.X. Study of Asphalt Behavior on Pre-Wet Aggregate Surface Based on Molecular Dynamics Simulation and Surface Energy Theory. *Coatings* **2023**, *13*, 1799. [[CrossRef](#)]
21. Xu, Y.X.; Chen, L.; Pei, F.; Chang, K.K.; Du, Y. Effect of the modulation ratio on the interface structure of TiAlN/TiN and TiAlN/ZrN multilayers: First-principles and experimental investigations. *Acta Mater.* **2017**, *130*, 281–288. [[CrossRef](#)]
22. Mulliken, R.S. Electronic population analysis on LCAO-MO molecular wave functions. *J. Chem. Phys.* **1955**, *23*, 1833–1840. [[CrossRef](#)]
23. Chibisova, M.A.; Chibisov, A.N.; Karpovich, N.F. Effect of bond population on the elasticity of tungsten nanowires: Ab initio calculation. *Comput. Mater. Sci.* **2016**, *114*, 99–101. [[CrossRef](#)]
24. Zhuo, L.C.; Zhao, Z.; Qin, Z.C.; Chen, Q.Y.; Liang, S.H.; Yang, X.; Wang, F. Enhanced mechanical and arc erosion resistant properties by homogeneously precipitated nanocrystalline fcc-Nb in the hierarchical W-Nb-Cu composite. *Compos. Part B* **2019**, *161*, 336–343. [[CrossRef](#)]
25. Adel, M.A.; Abdulrahman, I.A.; Hosam, H.; Penchal, R.M.; Mohamed, M.E.; Essam, A.; Waleed, H.E.; Teresa, D.G. Enhanced Corrosion Resistance and Surface Wettability of PVDF/ZnO and PVDF/TiO₂ Composite Coatings: A Comparative Study. *Coatings* **2023**, *13*, 1729. [[CrossRef](#)]
26. Li, H.Y.; Wang, X.H.; Guo, X.H.; Yang, X.H.; Liang, S.H. Material transfer behavior of AgTiB₂ and AgSnO₂ electrical contact materials under different currents. *Mater. Des.* **2017**, *114*, 139–148. [[CrossRef](#)]
27. Wu, Q.; Xu, G.F.; Yuan, M.; Wu, C. Influence of operation numbers on arc erosion of Ag/CuO electrical contact material. *J. Mater. Sci. Mater. Electron.* **2020**, *31*, 2497–2513. [[CrossRef](#)]
28. Li, H.Y.; Wang, X.H.; Hu, Z.D.; Qiu, Y.R. Effect of Ni addition on the arc-erosion behavior of Ag-4 wt.%SnO₂ electrical contact material. *J. Alloys Compd.* **2020**, *829*, 154487. [[CrossRef](#)]
29. Li, A.-K.; Chen, Y.-T.; Hu, J.-Q.; Wang, S.-B.; Chen, S.; Xie, M. Effect of Ni content on performance and arc behavior of AgNi electric contact material. *Chin. J. Nonferrous Met.* **2022**, *32*, 3746–3757. [[CrossRef](#)]
30. Zhang, Y.; Wang, J.Q.; Zhu, Y.C.; Cui, D.F.; Lu, N.Y. Study on Simulation and Experiment of Cu, C-Doped Ag/Ni Contact Materials. *Materials* **2022**, *15*, 4019. [[CrossRef](#)]

Disclaimer/Publisher's Note: The statements, opinions and data contained in all publications are solely those of the individual author(s) and contributor(s) and not of MDPI and/or the editor(s). MDPI and/or the editor(s) disclaim responsibility for any injury to people or property resulting from any ideas, methods, instructions or products referred to in the content.